Late Motor Decline After Accomplished Remyelination: Impact for Progressive Multiple Sclerosis

Natalia Manrique-Hoyos, MSc,[1] Tanja Jürgens, MSc,[2,3,4] Mads Grønborg, PhD,[5,6] Mario Kreutzfeldt, MSc,[2,3,4] Mariann Schedensack,[2,3] Tanja Kuhlmann, MD,[7] Christina Schrick,[2,3] Wolfgang Brück, MD,[2,3] Henning Urlaub, PhD,[6] Mikael Simons, MD,[1,8] and Doron Merkler, MD[2,3,4]

Objective: To investigate the impact of single or repeated episodes of reversible demyelination on long-term locomotor performance and neuroaxonal integrity, and to analyze the myelin proteome after remyelination and during aging.
Methods: Long-term locomotor performance of previously cuprizone-treated animals was monitored using the motor skill sequence (MOSS). Quantitative analysis of myelin proteome and histopathological analysis of neuronal/axonal integrity was performed after successful remyelination. Histopathological findings observed in experimental chronic remyelinated lesions were verified in chronic remyelinated lesions from multiple sclerosis (MS) patients.
Results: Following cessation of cuprizone treatment, animals showed an initial recovery of locomotor performance. However, long after remyelination was completed (approximately 6 months after the last demyelinating episode), locomotor performance again declined in remyelinated animals as compared to age-matched controls. This functional decline was accompanied by brain atrophy and callosal axonal loss. Furthermore, the number of acutely damaged amyloid precursor protein–positive (APP+) axons was still significantly elevated in long-term remyelinated animals as compared to age-matched controls. Confocal analysis revealed that a substantial proportion of these APP+ spheroids were ensheathed by myelin, a finding that was confirmed in the chronic remyelinated lesions of MS patients. Moreover, quantitative analysis of myelin proteome revealed that remyelinated myelin displays alterations in composition that are in some aspects similar to the myelin of older animals.
Interpretation: We propose that even after completed remyelination, axonal degeneration continues to progress at a low level, accumulating over time, and that once a threshold is passed axonal degeneration can become functionally apparent in the long-term. The presented model thus mimics some of the aspects of axonal degeneration in chronic progressive MS.

ANN NEUROL 2012;71:227–244

Multiple sclerosis (MS) is the most common disabling neurological disease in young adults (reviewed in Friese and colleagues,[1] Trapp and colleagues,[2] and Noseworthy and colleagues[3]). Disability often becomes apparent as a result of repeated attacks, followed by partial or complete remission of neurological symptoms (relapsing-remitting MS [RRMS]), which in turn is followed by a phase of gradually worsening clinical symptoms (secondary progressive MS [SPMS]). Moreover, some MS patients show a steady neurological decline even in the absence of acute attacks (primary progressive MS [PPMS]).

View this article online at wileyonlinelibrary.com. DOI: 10.1002/ana.22681

Received Nov 14, 2010, and in revised form Aug 26, 2011. Accepted for publication Nov 4, 2011.

Address correspondence to Dr Simons, Max-Planck-Institute of Experimental Medicine, Hermann-Rein Str. 3, 37075, Göttingen, Germany. E-mail: msimons@gwdg.de

M.S. and D.M. contributed equally to this work.

From the [1]Max Planck Institute for Experimental Medicine; [5]Department of Neurobiology, Max Planck Institute for Biophysical Chemistry, Göttingen, Germany; [6]Bioanalytical Mass Spectrometry Group, Max Planck Institute for Biophysical Chemistry, Germany; [2]Division of Clinical Pathology, Geneva University Hospital, Geneva, Switzerland; [3]Department of Pathology and Immunology, University of Geneva, Geneva, Switzerland; [4]Department of Neuropathology, University Medical Center, Georg August University, Göttingen, Germany; [8]Department of Neurology, University Medical Center, Georg August University, Göttingen, Germany; and [7]Institute of Neuropathology, University Hospital Münster, Münster, Germany.

Additional Supporting Information can be found in the online version of this article.

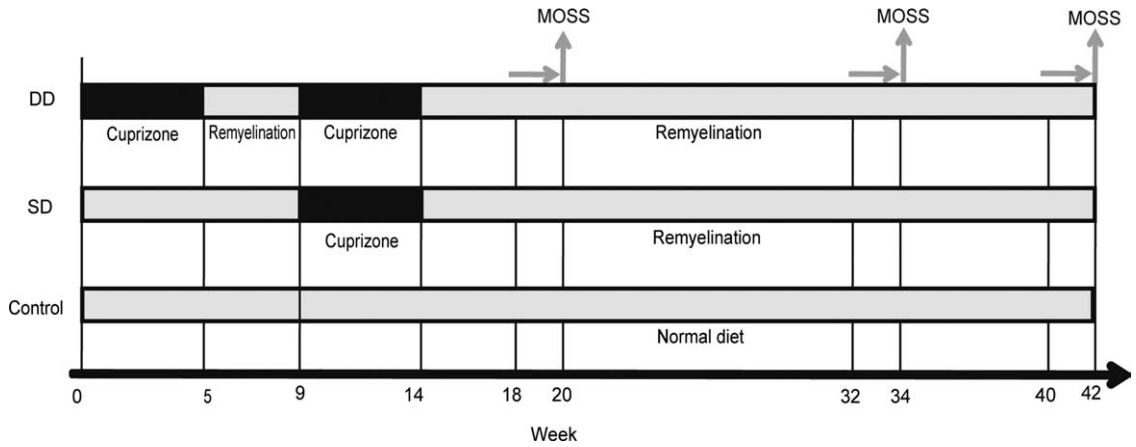

FIGURE 1: Experimental design of cuprizone treatment. Eight-week-old mice were fed cuprizone for 5 weeks, were then allowed to recover for 4 weeks, and finally received cuprizone for 5 more weeks (DD). A second group of mice (SD) were fed cuprizone for 5 weeks simultaneous to the second demyelination of the DD group as indicated. Animals were switched to a normal diet for 28 weeks until the end of the experiment. Age-matched controls were fed with a normal diet throughout the experiment. MOSS analysis was performed at the times indicated. Animals were first habituated to training wheels composed of regularly spaced crossbars for 2 weeks. Subsequently, running performance on complex wheels was recorded for an additional week. DD = double demyelination; MOSS = motor skill sequence; SD = single demyelination.

Supported by histopathological and magnetic resonance imaging (MRI) studies,[4,5] it appears clear that axonal loss is a key determinant of permanent disability in patients with MS. Acute axonal damage is most extensive in the early stages of the disease,[6] and the highest degree of acute axonal damage is associated with active demyelination.[7–9]

In addition to resolution of inflammation, remyelination can restore axonal conduction properties and is thought to contribute to the improvement of neurological function during remission in RRMS.[10,11] However, since the disability is permanent and irreversible in the progressive phase, it is important to elucidate what determines the transition into this stage. The accumulation of noncompensable axonal loss mediated by inflammatory processes may explain the development into a progressive form of the disease. Indeed, inflammatory infiltrates were invariably associated with axonal damage, not only in RRMS but also in chronic progressive MS.[12] However, it is still poorly understood why current immunomodulatory treatment reduces the relapse rate but does not prevent the increasingly permanent neurological deficits in progressive MS. One explanation might be that inflammatory cells are trapped behind an intact blood–brain barrier in progressive MS and are thus no longer accessible to the therapeutic treatment. A further explanation may, however, be that ongoing degeneration does not solely rely on inflammation.[13,14]

Age is an important risk factor for MS progression.[10,11] Studies have shown that the progressive phase is an age-dependent process, starting at a mean age of 39 years.[15] Regardless of the disease subtype—primary progressive multiple sclerosis (PPMS), secondary progressive multiple sclerosis (SPMS), or 1 relapse followed by progression—the average age at which patients enter the progressive stage is strikingly similar.[15] In addition, once a clinical threshold of disability is reached, the number of relapses is not prognostic for the further clinical course.[16] This raises the possibility that age-related processes are relevant for the initiation of the progressive phase of the disease.

Here we studied the long-term functional impact of demyelination in the C57BL6 cuprizone mouse model of MS.[17–19] We provide evidence that after a phase of initial functional recovery, locomotor decline occurred long after completed remyelination. This suggests that mechanisms operating indepently of acute inflammation may also contribute to the long-term disability and may be of importance for our understanding of disease progression in MS.

Subjects and Methods

Mice and Cuprizone Treatment

Eight-week-old C57Bl6 mice were assigned to 3 groups, namely double demyelination (DD), single demyelination (SD), and control (see also Fig 1). DD animals were fed with 0.25% cuprizone (Sigma, St. Louis, MO) in milled chow for 5 weeks, followed by a normal diet for 4 weeks. Subsequently, they received a 0.25% cuprizone diet for 5 weeks, which was then replaced by a normal diet for the rest of the experiment. Animals in the SD group received a normal diet for 9 weeks (until the start of the second demyelinating event of group DD), were then fed with 0.25% cuprizone for 5 weeks, and finally were fed with a normal diet for the rest of the experiment. Age-matched controls received a normal diet throughout the experiment.

Motor Skill Sequence

Assessment of motor performance following remyelination was carried out as previously described using the motor skill sequence (MOSS).[20] Separate analyses were performed 6, 20, and 28 weeks after cuprizone removal from the diet (see Fig 1). For every MOSS session, each animal was transferred to an individual cage and was allowed to run voluntarily on a training wheel with regularly spaced crossbars for 14 days. Subsequently, the wheel was replaced by a "complex" wheel containing irregularly-spaced crossbars and the animals were allowed to run voluntarily for 7 consecutive days. The following parameters were monitored continuously: maximum running velocity in revolutions/min (V_{max}), accumulated distance in meters ($Dist_{ac}$), number of individual runs (N_{run}), accumulated running time (T_{total}), and maximum distance per run ($Dist_{max}$). $Dist_{ac}$, T_{total}, and N_{run} represent the values accumulated during the last 24 hours, whereas V_{max} and $Dist_{max}$ represent the maximum values achieved during that time.

Human Brain Tissue

Human brain autopsies of MS patients were obtained from the Department of Neuropathology collection at the University Medical Center Göttingen. Their use for scientific purposes was approved by the ethics committee of the University of Göttingen (Göttingen, Germany).

Histology

Animals were sedated with a 14% chloral hydrate intraperitoneal injection, perfused transcardially, brain were fixed with 4% paraformaldehyde (PFA). Tissue was processed and embedded in paraffin as described[21,22] to obtain 1μm-thick coronal and sagittal sections. Luxol fast blue–periodic acid Schiff (LFB-PAS) staining was performed to assess the extent of demyelination according to a standardized score ranging from 0 (no demyelination) to 3 (complete demyelination).[23]

Immunohistochemistry was performed using antibodies against activated microglia/macrophages (Mac3 clone M3/84; BD Bioscience, NY, USA), astrocytes (glial fibrillary acidic protein [GFAP] clone 6F2; Dako, Hamburg, Germany), neuronal nuclei (NeuN; Chemicon, Temecula, CA), axonal damage with amyloid precursor protein (APP, clone 22C11; Chemicon), and myelin basic protein (MBP, A0623; Dako), followed by labeling with biotinylated secondary antibodies. Avidin-biotin technique with 3,3-diaminobenzidine was used for visualization. Fluorescent immunohistochemistry was performed for APP, MBP, and neurofilament 200 (NF200, clone N52; Sigma) with Cy2-conjugated donkey anti-mouse immunoglobulin G (IgG) and Cy3-conjugated goat anti-rabbit IgG secondary antibodies (Jackson ImmunoResearch Laboratories, Suffolk, UK). Histological sections stained with anti-APP, Mac3, NeuN, and GFAP antibody, and counterstained with haemalum were scanned using the Dotslide System (Olympus GmbH, Hamburg, Germany), coupled to an Olympus BX51 microscope.

For axonal counting on sagittally cut sections paraffin-embedded sections were stained against neurofilament (1:600; monoclonal mouse anti-human neurofilament protein, clone 2F11, Dako M0762; Dako) and detected with a secondary fluorescent-labeled antibody (1:200; Alexa Fluor®555 goat anti-mouse IgG1, Invitrogen A21127; Invitrogen, NY, USA). Tissue was counterstained with DAPI nucleic acid stain (1:10,000; D3571; Invitrogen) and sections were coverslipped with Fluoprep (bioMérieux).

Axonal densities of corpus callosum were assessed by 2 independent methods:

1. Densitometric measurements of callosal axons were performed on coronal NF200-stained sections. Images were obtained at each side of the midsagittal line of the corpus callosum under equal acquisition parameters with a confocal microscope (LSM 510; Carl Zeiss MicroImaging, Inc., Göttingen, Germany or TCS SP2 AOBS; Leica, Solms, Germany) and the signal intensity was analyzed with Image J. To examine whether APP+ axons were myelinated, fluorescence immunohistochemistry of sagittal sections of the corpus callosum was performed with APP and MBP antibodies, and the presence of an MBP-positive signal surrounding APP was determined.
2. Callosal axons were evaluated on sagittal neurofilament-stained brain sections. Images of transversally cut axons were obtained by a Zeiss LSM 510 laser scanning microscope coupled to a Zeiss Axiovert 100 M inverted microscope equipped with a ×63/1.4 oil immersion objective. Callosal axons were captured in 3 to 5 randomly selected, non-overlapping areas ($146.2 \times 146.2\mu m^2$) per animal. Confocal stacks (thickness of 1.2–3.7μm; interval of 0.41μm) were scanned in the z-direction (Software LSM 510; Zeiss) and 3 to 5 overlapping stacks composed 1 layer using Fiji. We counted axons in an area of at least $5{,}600\mu m^2$ per animal using a custom-programmed script in Cognition Network Language–based on the Definiens Cognition Network Technology platform (Definiens Developer XD software; Definiens AG, Munich, Germany). The Cognition Network Language is an object-based procedural computer language which is specifically designed for automated analysis of complex, context-dependent image analysis tasks.[24] In brief, neurofilament-positive axons were detected based on their contrast to the image background signal. To adapt for potential variable background staining levels, the area surrounding potential axonal structures was segmented and the mean intensity difference between the structures was calculated. Neurofilament-positive structures displaying a signal difference higher than 8 from their surroundings were classified as axons (for detailed formula see the Definiens Developer XD 1.5.2 Reference book). Complementary, adjacent sections were stained using Bielschowsky's silver impregnation technique and sections were scanned using Zeiss Mirax Virtual Slide Scanner (Carl Zeiss MicroImaging GmbH). The thickness of the corpus callosum was then measured using a Mirax Slide Viewer (Carl Zeiss MicroImaging GmbH). Axonal numbers were subsequently calculated by multiplying axonal densities (expressed as axons per square millimeter) with the thickness of the corpus callosum of a given animal.

Human Tissue Staining

Histopathological analysis was performed on PFA-fixed sections from brain autopsies of patients with documented progressive MS. All tissue blocks (n = 6 blocks from 4 patients) were selected if signs of remyelination (judged by LFB/PAS staining) were observed. Fluorescence immunohistochemistry was performed for MBP and APP.

Analysis of Neuronal Numbers

Sections stained for neuronal nuclei with NeuN antibodies were scanned. Neuronal numbers were automatically counted using a script in Cognition Network Language based on the Definiens Cognition Network Technology platform. Briefly, the cortical region of interest was drawn manually and NeuN-positive cells were detected based on color criteria. After finer segmentation to discriminate between nucleus and cytoplasm, the object was classified as a NeuN-positive cell if the soma was below a certain size and had 0 to 1 nuclei. If more than 1 nucleus was detected within 1 soma, the object was split using each nucleus as seed to grow into the surrounding cytoplasm, stopping if growing borders converged or the cytoplasmic border was reached. Finally, the total number and density of NeuN-positive cells was calculated.

Statistical Analysis

Two-factorial repeated measurements analysis of variance (ANOVA) was performed to analyze wheel-running performance (MOSS), with treatment and time course as independent variables and the respective wheel-running parameter as a dependent variable. If ANOVA indicated significant differences for the main effect of treatment, Fisher's least significant difference (LSD) post hoc test was applied. Values are expressed as mean ± standard error of the mean (SEM). For histological analysis, a 1-way ANOVA was performed, followed by a Tukey test or Fisher's LSD test for pairwise comparisons, where appropriate. For comparison between 2 samples, a Student t test was applied. A p of <0.05 was considered significant in all tests. Statistics were calculated using SPSS 11.0 (SPSS, Inc., Chicago, IL) or SigmaPlot software (Systat Software, Inc., Chicago, IL).

Electron Microscopy

Electron microscopy was performed according to a modified protocol as described.[21] Briefly, mice were fixed by transcardial perfusion with 4% PFA and 2.5% glutaraldehyde in 0.1M phosphate buffer containing 0.5% NaCl. The tissue was embedded in Epon, the corpus callosum was cut and stained with toluidine blue, and ultrathin sections were cut and treated with uranyl acetate and lead citrate. The sample area was selected at low magnification in the electron microscope (×2,500) before systematically recording images at ×16,000 magnification using a CCD camera (MegaView III, Soft Imaging System). Axon diameters and myelin sheath thicknesses of at least 300 axons (>0.35μm in diameter) were measured from each animal using CellF software (Olympus Soft Imaging Solutions GmbH, Germany), to calculate the g-ratio (axon diameter/fiber diameter) as described.[25]

Proteomic Analysis of Myelin

Animal experiments were conducted in accordance with animal protection laws approved by the Government of Lower Saxony, Germany. Three young (12 weeks old) and 3 old (over 20 months old) C57BL/6J mice were sacrificed by cervical dislocation and their complete brains were extracted and frozen. In addition, 8-week-old C57BL/6J mice were fed for 6 weeks with 0.2% cuprizone mixed in normal chow, followed by 6 weeks of normal diet. Samples of the corpus callosum of the cuprizone-fed and age-matched control mice were obtained and frozen.

Myelin Isolation and Purification

Myelin was isolated according to a modified protocol as previously described[26] to obtain purified myelin. All steps were performed on ice in a SW41 Ti rotor with an Optima XL-70 ultracentrifuge (Beckman Coulter, Krefeld, Germany) and the protein concentration of the myelin preparation was measured with the Bradford method.[27]

Sample Preparation, Isobaric Tags for Relative and Absolute Quantitation Labeling and Strong Cation Exchange Fractionation

Equal amounts of purified myelin (15μg for young and old samples, and 8μg for remyelinated and control samples) were resuspended in 0.85% RapiGest in 50mM triethylammonium bicarbonate (TEAB), treated with reducing agent (isobaric tags for relative and absolute quantitation [iTRAQ] Reagents Multiplex Kit, Applied Biosystems, Carlsbad, USA) and alkylated with iodoacetamide. After trypsin digestion, peptides labeled with iTRAQ reagents were pooled together in pairs (young vs old and remyelinated vs control). Each pooled sample was separated by strong cation exchange (SCX) fractionation (ICAT Cartridge Kit; Applied Biosystems), eluted stepwise by 300μl injection of KCl solutions (5–1,000mM, 25% acetonitrile, and pH 2.7–3.0). Further purification and desalting was performed on a reverse-phase microcolumn, as described.[28]

Mass Spectrometry and Analysis

Purified myelin samples from young and old mice as well as remyelinated animals and their age-matched controls were analyzed by liquid chromatography coupled to tandem mass spectrometry (LC-MS/MS). Each purified sample was injected onto a C18 reverse-phase column (Reprosil; Maisch, Germany) and eluted at 200nl/min with different mobile phase B concentrations (7–40%) in an 80% acetonitrile and 0.15% formic acid solution. Mass spectrometry analysis of the digested peptides was carried out using a Thermo LTQ XL Orbitrap (Thermo Fisher Scientific, Bremen, Germany) coupled to an Agilent 1100 series LC system. Peak lists were searched against the National Center for Biotechnology Information (NCBI) nonredundant reference sequence (RefSeq) database (http://www.ncbi.nlm.nih.gov/RefSeq)[29] using Mascot v.2.2 as a search engine (Matrix Science, Boston, MA).[30] Mass accuracy was 5ppm for both parent ion and fragment ions. The peptides were constrained to be tryptic with a maximum of 2 missed cleavages. Only proteins with a Mascot score over 25 were

considered in the data set. To correct for a bias due to unequal protein mixing, the data set was normalized by dividing the raw peptide ratios with their median value, which resulted in a balanced distribution at a ratio of approximately 1:1. Proteins identified from peptides with a ratio >1.2 or <0.8 can be considered differentially expressed, as described.[31–34] The possible localization and function of proteins was determined using the UniProt Knowledgebase (UniProtKB) protein database (http://www.uniprot.org/help/uniprotkb).[35] Transmembrane proteins were predicted using the TMHMM2.0 (Krogh and colleagues[36]) or Phobius software.[37]

Results

We examined the long-term impact of cuprizone-induced demyelination and remyelination using the following paradigm (see scheme of Fig 1 for experimental design): a first group of mice was subjected to DD by feeding 8-week-old mice with cuprizone for 5 weeks and allowing them to recover for 4 weeks before cuprizone treatment was repeated for 5 more weeks. A second group of mice (SD) were fed once with cuprizone for 5 weeks, simultaneously with DD group's second exposure to cuprizone. Thereafter, animals of both DD and SD groups were fed normal diets for 28 weeks. Age-matched controls were fed a normal diet throughout the experiment.

Locomotor performance was assessed using MOSS analysis within a time span of ~6 months at 3 different time points following discontinuation of cuprizone (see Fig 1). MOSS is an automated complex wheel test particularly suited to detect latent motor deficits after cuprizone-induced demyelination.[20,38] Six weeks after cuprizone removal, both treated groups (SD and DD) exhibited similar locomotor performance in parameters reflecting general motivation and fitness (N_{run}, T_{total}, and $Dist_{ac}$; Fig 2, left panel) compared to age-matched controls. However, V_{max} and D_{max} were still significantly reduced in both groups compared to age-matched controls. Previous studies suggested that reduced maximal running performances were related to impaired capacity of complex bihemispherical motor coordination.[39] Furthermore, these findings were congruent with earlier findings showing that motor deficits are still evident after 6 weeks of recovery following a cuprizone diet.[20,38] We re-examined the animals 14 weeks later (ie, 20 weeks of recovery), and in contrast to the first MOSS measurement, locomotor performance of remyelinated animals was indistinguishable from age-matched controls. These results indicate that remyelination, probably in combination with neuroplastic processes, can restore locomotor function in the medium-term following demyelination. To further investigate whether functional recovery remained stable in the long term, we repeated MOSS analysis 28 weeks after stopping cuprizone. At this final time point, remyelinated animals (irrespective of single or repeated prior exposure to cuprizone) displayed deteriorated locomotor performance as compared to age-matched controls in V_{max} and D_{max} (see Fig 2, right panel). In contrast, no differences were detected in wheel-running parameters assessing motivation and/or fitness in animals previously treated with cuprizone compared to controls. Similarly, no differences in any of the locomotor parameters measured by MOSS were observed between single and double cuprizone-treated groups. These data showed that mice can completely recover following cuprizone treatment, but redevelop late-onset functional deficits.

In parallel, we performed histomorphologic analysis in a subset of animals that were treated in the same manner as the mice used for MOSS measurements. Callosal demyelination was first evaluated according to a standardized score from 0 (no demyelination) to 3 (complete demyelination) on LFB/PAS–stained coronal sections.[23] Consistent demyelination of the corpus callosum following 5 weeks of cuprizone feeding was observed (see Fig 3). LFB/PAS analysis furthermore indicated that demyelination was, to a large extent, reversible in animals subsequently exposed for 28 weeks to a normal diet (see Fig 3B). To assess remyelination on an individual axonal level, we performed electron microscopic examination, which is the gold standard for the evaluation of remyelination.[40] We determined the fraction of nonmyelinated fibers in percentage of total fibers and calculated the g-ratio (axon diameter/fiber diameter) (Fig 4A–C). One-way ANOVA indicated significant differences between the experimental groups tested with regard to the g-ratio ($p < 0.01$) and percentage of unmyelinated fibers ($p < 0.05$). Post hoc analysis further revealed statistically significant differences in the g-ratio when comparing the control group to the remyelinating groups at 6 weeks or the DD group at 28 weeks, respectively (6 weeks: 0.80 ± 0.008, DD: 0.8 ± 0.012, control: 0.73 ± 0.010). In contrast, no significant difference of the g-ratio was noted when comparing the different remyelinating groups. Similarly, the percentage of unmyelinated fibers was significantly ($p < 0.05$) elevated in the DD group (26 ± 8.8%) and the 6-week group (23 ± 2.6%) as compared to the control group (5.9 ± 1.2%). No significant difference was found in the percentage of unmyelinated fibers when comparing the different remyelinated groups to each other (6 weeks, 28-week SD, and 28-week DD). Furthermore, a trend, but not a statistically significant difference, was observed when comparing the SD group to the control group with regard to percentage of unmyelinated

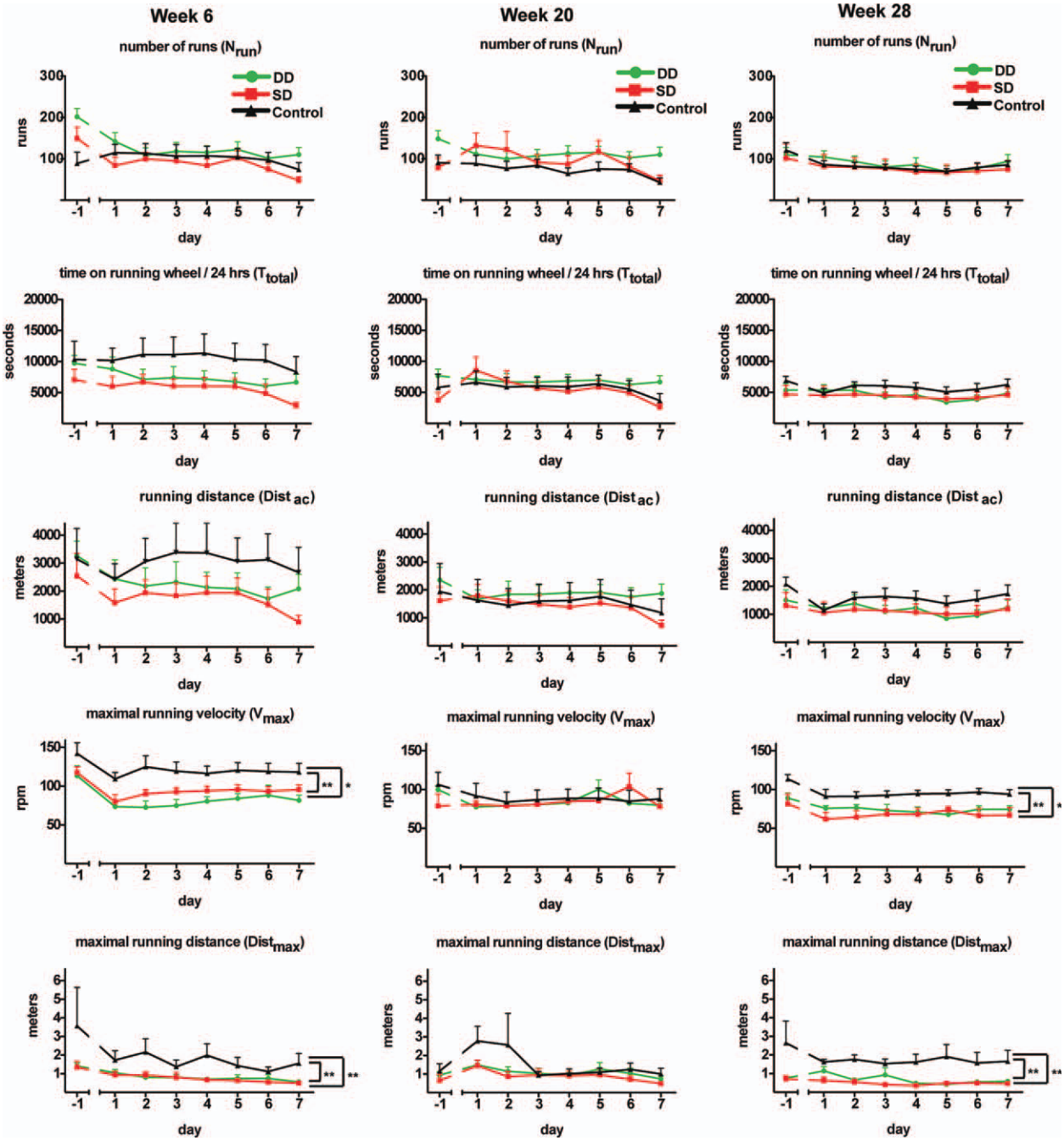

FIGURE 2: Late-onset latent motor deficits as measured by wheel-running performance after remyelination. Animals received 1 (*red*) and 2 (*green*) cycles of cuprizone to induce demyelination and were allowed to recover for 28 weeks, during which MOSS performance was compared to age- and sex-matched controls (*black*). Recording was preceded by a 2-week training session (day −1: performance of last day on training wheels, for details see Subjects and Methods). Complex wheel performance (days 1 to 7) is shown as follows: 6 weeks (left panels), 20 weeks (central panels), and 28 weeks (right panels) after cuprizone withdrawal. Differences between the cuprizone and control group with regard to wheel-running performance were calculated by repeated measurements ANOVA. If ANOVA indicated significant differences in the main effect ($p < 0.05$), Fisher's LSD post hoc tests were applied. *$p < 0.05$, **$p < 0.01$, rpm: revolutions per minute (n = 8–12 animals per group). ANOVA = analysis of variance; DD = double demyelination; $Dist_{ac}$ = distance in meters accumulated in 24 hours; $Dist_{max}$ = maximum distance per run; LSD = lest significant difference; MOSS = motor skill sequence; N_{run} = number of individual runs in 24 hours; SD = single demyelination; T_{total} = accumulated running time in 24 hours; V_{max} = maximum running velocity in revolutions per minute in 24 hours.

fibers (20 ± 8.4%, $p = 0.068$) and the g-ratio (0.77 ± 0.018, $p = 0.12$) due to the slightly higher variability of recorded values in the DD group.

We also evaluated axonal densities and axonal numbers in the corpus callosum using 2 independent methods. First, axons were immunohistochemically visualized

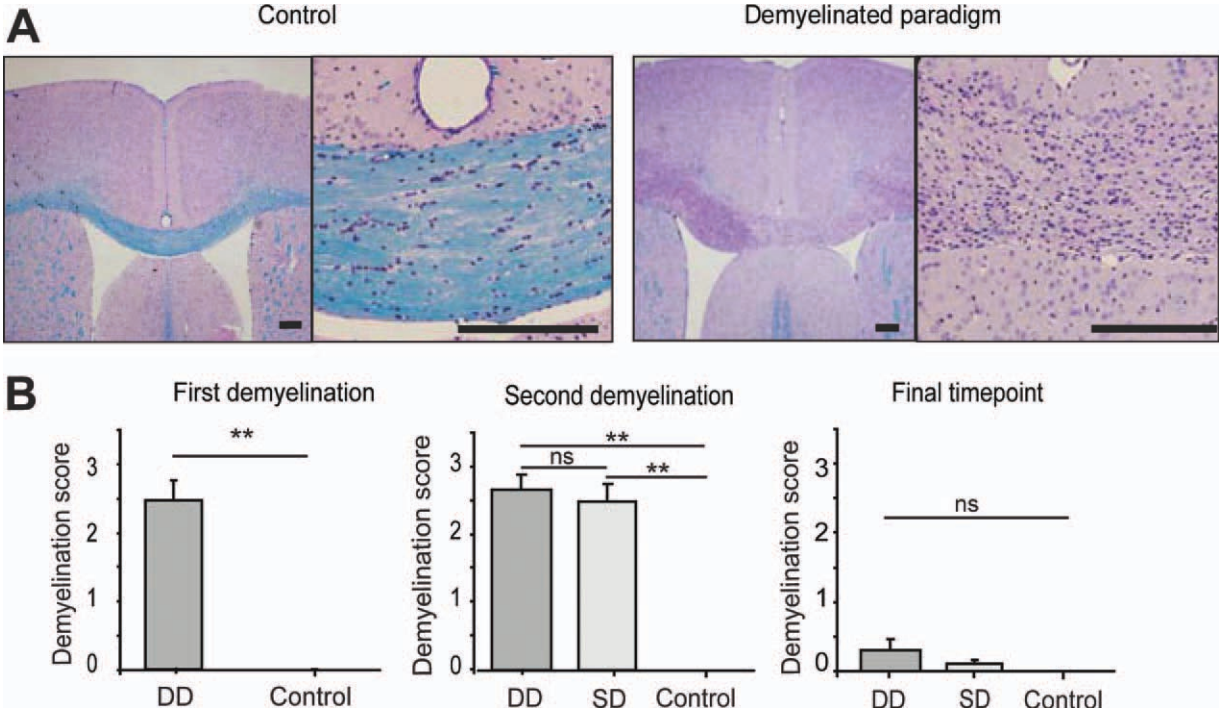

FIGURE 3: Cuprizone-induced demyelination and remyelination. (A) Representative LFB/PAS–stained corpus callosum of untreated control (left) and after 5 weeks of cuprizone treatment (right). Extensive callosal demyelination is evident in the right panel. Bar = 200μm. (B) Semiquantitative analysis of callosal demyelination (n = 3–9 animals per group) and compared to age-matched control (n = 2–6). A score of 3 corresponds to maximal demyelination, a score of 0 represents no detectable demyelination. For the first demyelination (left), a *t* test was applied. For second demyelination (center) and final time point (right), if ANOVA indicated significant differences in the main effect ($p < 0.05$), Tukey test pairwise comparison was applied. **$p < 0.01$. Data shown as mean ± SEM. First demyelination: week 5, second demyelination: week 14, final time point: week 42 (see also Fig 1A). ANOVA = analysis of variance; DD = double demyelination, LFB/PAS = Luxol fast blue/periodic acid Schiff; SD = single demyelination; SEM = standard error of the mean. [Color figure can be viewed in the online issue, which is available at www.annalsofneurology.org.]

on coronal sections and relative axonal densities were determined by densitometry (Fig 5A–D). This analysis revealed a substantial axonal loss in animals that remyelinated for 28 weeks as compared to untreated controls (see Fig 5D). Second, we quantified the numbers of crossing fibers on sagittally cut sections during advanced remyelination (3 weeks of remyelination) and after terminated remyelination 6 weeks and 28 weeks after stopping cuprizone. In doing so, we found a significant drop in axonal numbers in the corpus callosum during ongoing remyelination (3 weeks vs 6 weeks after stopping cuprizone) and following completed remyelination (6 weeks vs 28 weeks of remyelination). Together, these results show that a low degree of axonal degeneration continued even after remyelination had been accomplished. In parallel to these analyses, we noted a moderate but significant increase in activated microglia and astrocyte density in remyelinated animals as compared to age-matched controls at the final time point (Supplementary Fig S1).

To further evaluate ongoing axonal damage in the late stages, we determined APP levels in the axons at 28 weeks after cuprizone removal. Previous studies have shown that axonal accumulation of APP represents a reliable measure of acute axonal injury. Time-lapse imaging has revealed that APP accumulates locally in a damaged axon, where it can either disappear because the axon degenerates or disappear because axonal transport is restored.[24] Strikingly, APP-positive axons were still detectable in the corpus callosum of mice that were fed with cuprizone 6 months before, but virtually absent in control animals (Fig 6A,B). Together, these data strongly support our conclusion that axonal damage, and probably also degeneration, continue long after the demyelinating trigger has been removed.

To determine the proportion of unmyelinated vs myelinated axons showing axonal dysfunction, sagittal sections of the corpus callosum were double-stained for APP and MBP. Interestingly, a significant fraction (19% for DD and 27% for SD) of APP-positive axons was ensheathed by MBP-positive myelin (see Fig 6C,D). To verify whether this also occurs in MS, we performed similar staining on autopsy lesions showing extensive remyelination and with a documented long clinical history of progressive MS (n = 6 lesions of 4 MS cases, average disease duration 17.2 ± 4.7 years). Similarly, we found

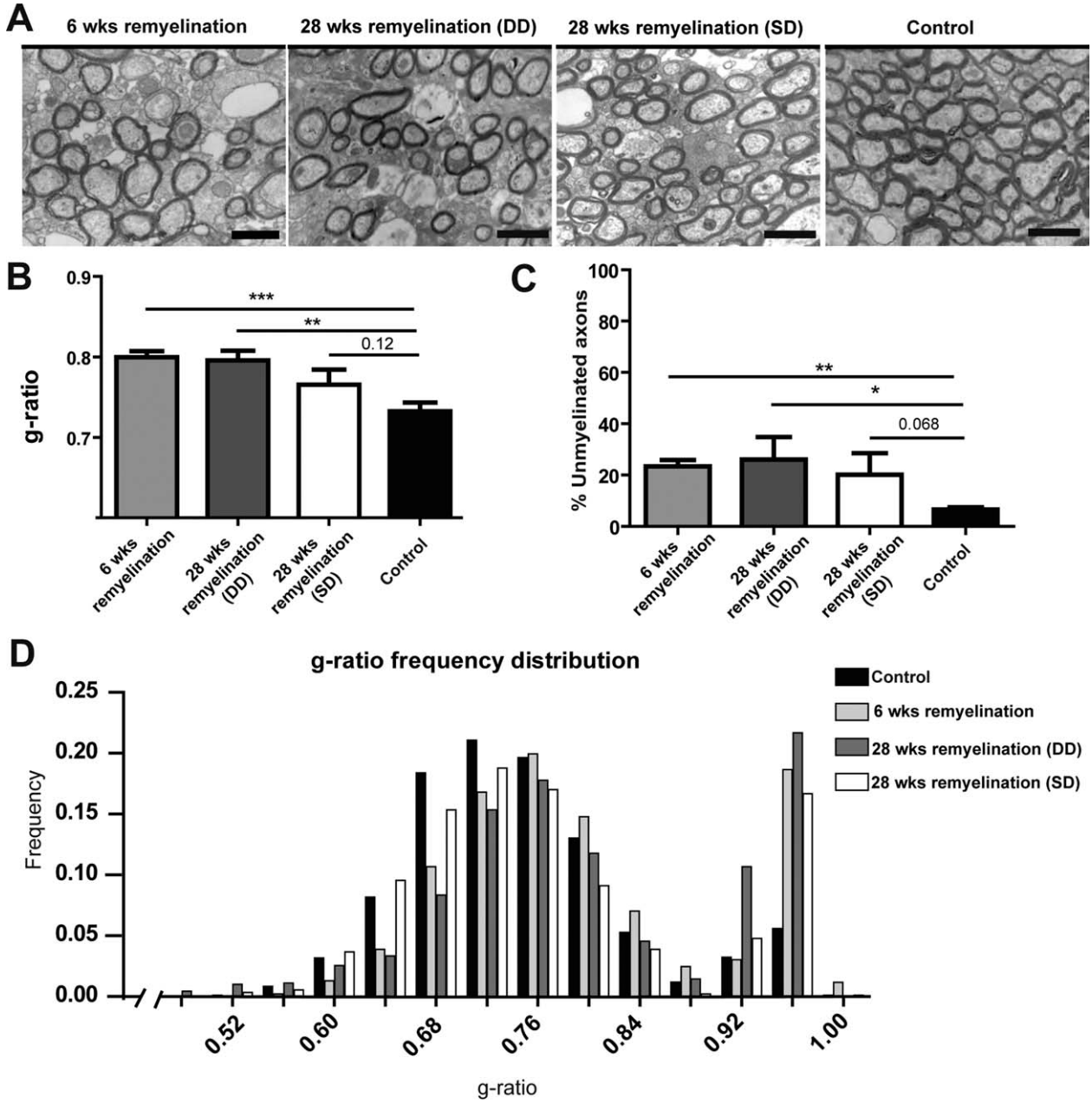

FIGURE 4: Ultrastructural analysis of long-term effects of cuprizone-induced demyelination of myelin in corpus callosum. (A) Electron microscopy of the corpus callosum after 6 weeks of remyelination, as well as after 28 weeks of recovery for DD, SD, and control animals are shown. Bar = 1 μm (B) Axonal diameter to the fiber diameter (g-ratio) in treated groups and controls is shown as the mean ± SEM. (C) Percentage of nonmyelinated fibers as compared to controls (mean ± SEM). (D) Distribution of g-ratio of all axons in the treated and control groups. n = 3–11 animals per group, >300 axons >350nm in diameter per animal. DD = double demyelinated; SD = single demyelinated; SEM = standard error of the mean.

APP-positive axons in remyelinated lesions, and the fraction of myelin-ensheathed, APP-positive axons was 14%, thus confirming our results obtained in remyelinated animals following cuprizone treatment (see Fig 6E,F).

Several studies have highlighted the importance of brain atrophy in permanent neurological impairment.[41–44] We evaluated the cortical thickness of coronal sections 28 weeks after stopping cuprizone (week 42; see Fig 1) in 3 different regions: medial, paramedial, and lateral (Fig 7D). Whereas the medial and lateral regions showed no differences in cortical thickness (ANOVA, $p > 0.05$), a significant decrease was detected in the paramedial region (ANOVA, $p < 0.01$) (see Fig 7E–G). In addition, we observed a marked reduction of corpus callosum thickness in the medial region. To determine whether cortical neuronal loss occurred, we performed an automated analysis of total neuronal numbers in a defined cortical area at week 42

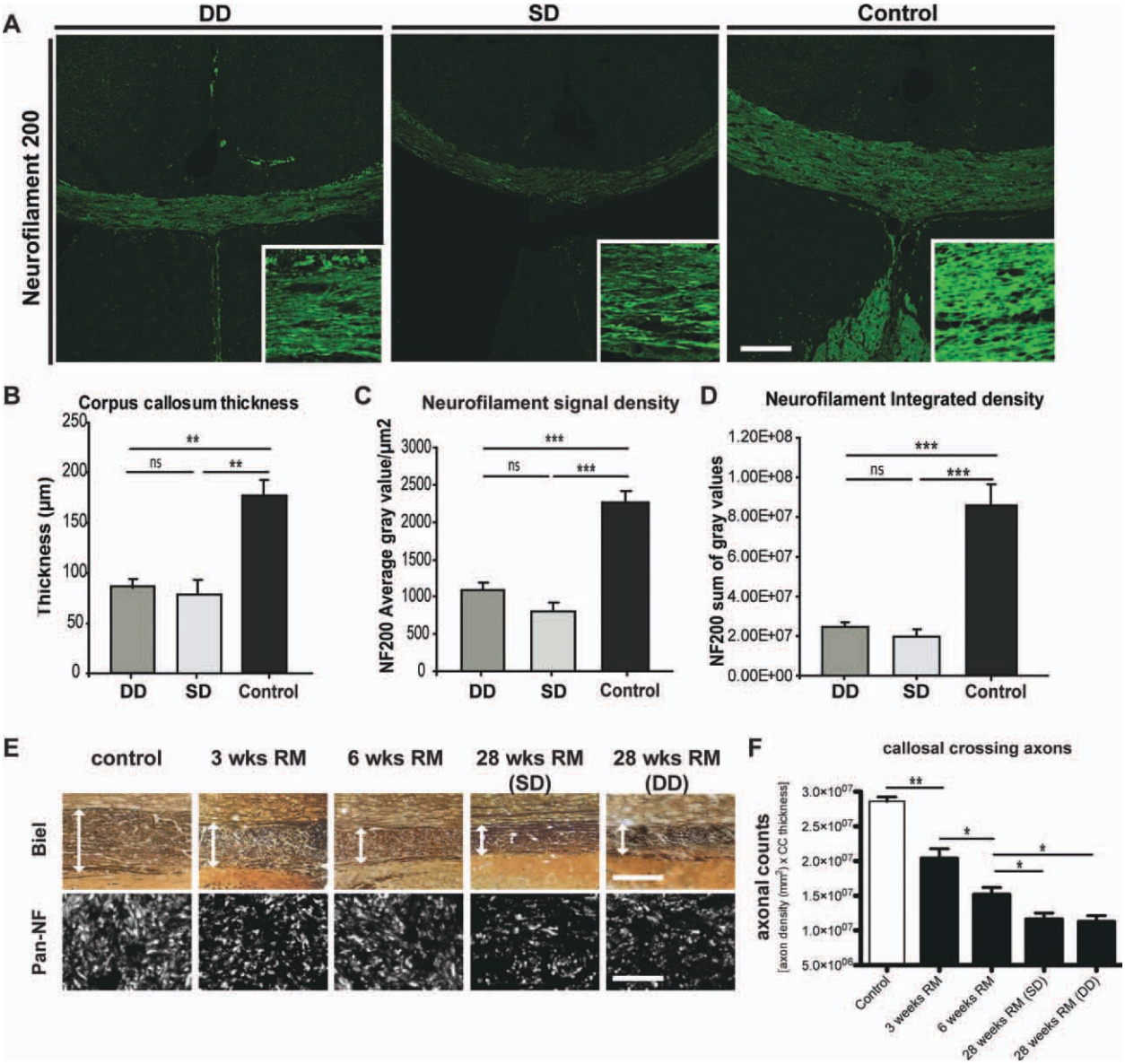

FIGURE 5: Cuprizone-induced demyelination results in axonal loss and corpus callosum atrophy, as seen 28 weeks after cuprizone treatment removal. (A) Representative images (overview: ×100, insets: ×400 magnification) of coronal sections stained for NF200 from DD, SD, and control animals are shown. Insets show high magnification of NF200. (B) Quantitative analysis of corpus callosum thickness as determined by MBP staining and image analysis. (C) Mean and (D) integrated density of NF200 signal in the corpus callosum of the different groups is shown as the mean ± SEM (n = 5–9). Statistically significant differences are indicated by asterisks. If ANOVA indicated significant differences in the main effect ($p < 0.05$), Tukey test pairwise comparison was applied (*$p < 0.05$, **$p < 0.01$, ***$p < 0.001$). (E) Upper panel: The thickness of the CC was determined on sections stained by Biel (extent of CC indicated by double arrows). Lower panel: Axonal densities were determined on confocal images of PAN-NF–stained adjacent sections within CC. (F) Callosal axonal numbers were calculated by multiplying axonal densities (expressed as axons per square millimeter) by the thickness CC of a given animal. Bars = mean ± SEM. Statistically significant differences are indicated by asterisks. If ANOVA indicated significant differences in the main effect ($p < 0.05$), Tukey test pairwise comparison was applied (*$p < 0.05$, **$p < 0.01$, ***$p < 0.001$). Bar in A = 100μm; upper row in E = 120μm, lower row in E = 25μm. ANOVA = analysis of variance; Biel = Bielschowsky's silver impregnation; CC = corpus callosum; DD = double demyelinated; NF200 = neurofilament 200; MBP = myelin basic protein; ns = not significant; PAN-NF = pan-neurofilament; RM = remyelination; SD = single demyelinated; SEM = standard error of the mean; wks = weeks.

in comparison to age-matched controls. For this purpose, neuronal nuclei in coronal sections were stained with NeuN antibodies, scanned, and NeuN-positive cells were counted automatically (for details see Subjects and Methods). However, no differences in total neuronal numbers or density were found between any of the groups (see Fig 7B). Together, our results indicate that the insult preferentially affected axonal processes but

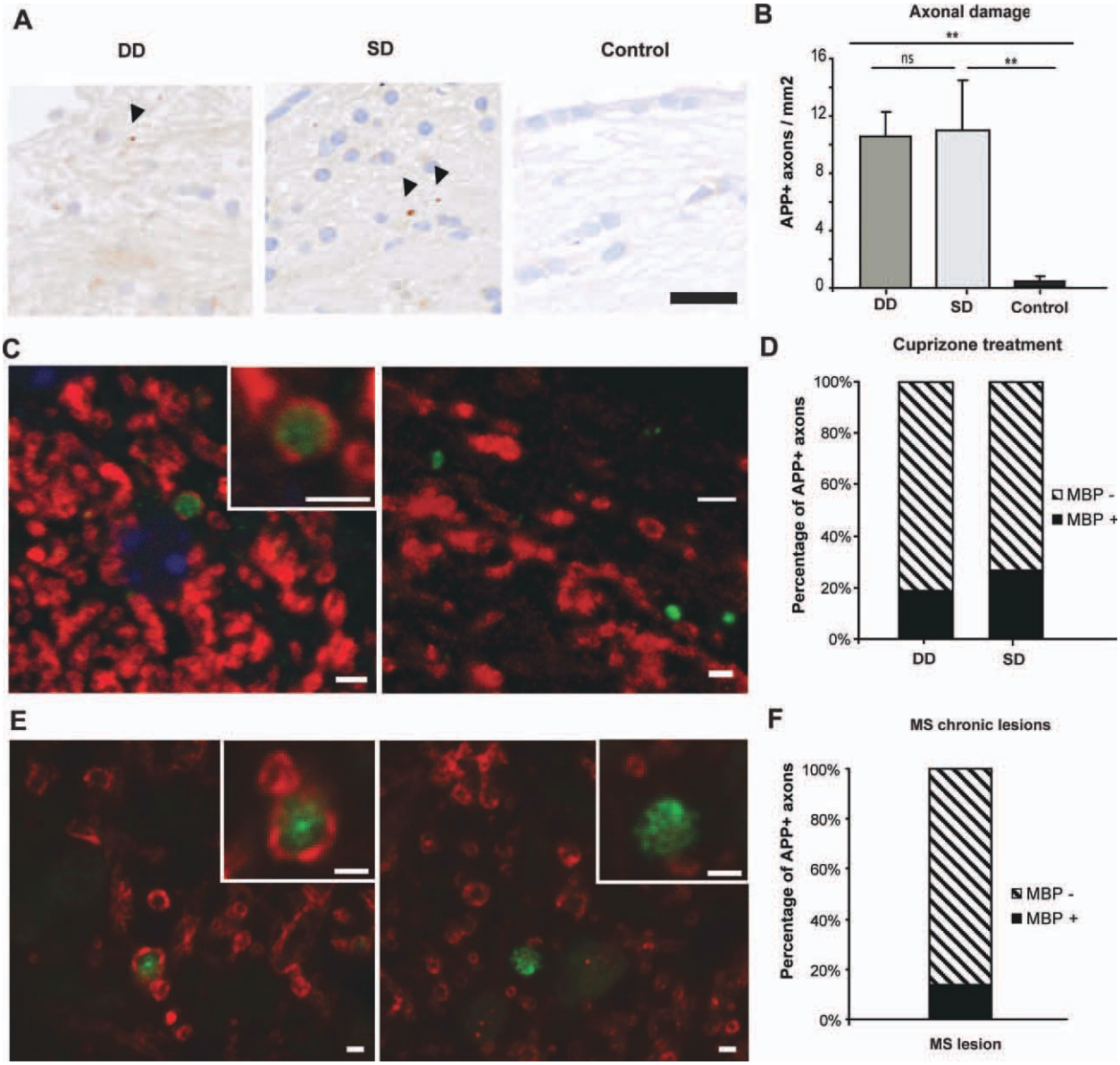

FIGURE 6: APP-positive axons can be detected in chronic remyelinated lesions. (A) Coronal sections were analyzed in the medial part of the corpus callosum by immunohistochemistry with an antibody against APP. Arrowheads indicate examples of APP-positive structures. Bar = 20μm. (B) Quantification of APP-positive axons in central corpus callosum. Statistically significant differences are indicated by asterisks; if ANOVA indicated significant differences in the main effect ($p < 0.05$), Tukey test pairwise comparison was applied ($p < 0.01$). (C) Sections were stained by immunohistochemistry with antibodies against APP and MBP. Left image shows an example of an MBP-positive ring surrounding an APP-positive axon. Right image displays an example of an APP-positive axon lacking MBP. Bar = 2μm. (D) Quantification of the percentage of myelinated and unmyelinated APP-positive axons in central corpus callosum of cuprizone-treated groups (n = 5–9 per group). (E) MS autopsy lesions showing extensive remyelination and with known long clinical history of progressive MS (average disease duration 17.2± 4.7 years) were stained by immunohistochemistry with antibodies against APP and MBP. Left image shows an example of an MBP-positive ring surrounding an APP-positive axon. Right image displays an example of an APP-positive axon lacking MBP. Bar = 2μm. (F) Quantification of the percentage of myelinated and unmyelinated APP-positive axons in lesions of progressive MS patients (n = 5 MS cases). ANOVA = analysis of variance; APP = amyloid precursor protein; DD = double demyelination group; MBP = myelin basic protein; MS = multiple sclerosis; SD = single demyelination group.**

did not cause substantial loss of neuronal somas in the cerebral cortex.

Changes in myelin composition can induce axonal pathology.[45–47] Therefore, proteome analysis was designed as an exploratory approach to unravel tangible quantitative differences in myelin protein composition following remyelination compared to controls. In addition, we analyzed how myelin changes its composition in older animals (20 months old). Myelin was prepared from ~12-week-old and ~20-month-old mice, from

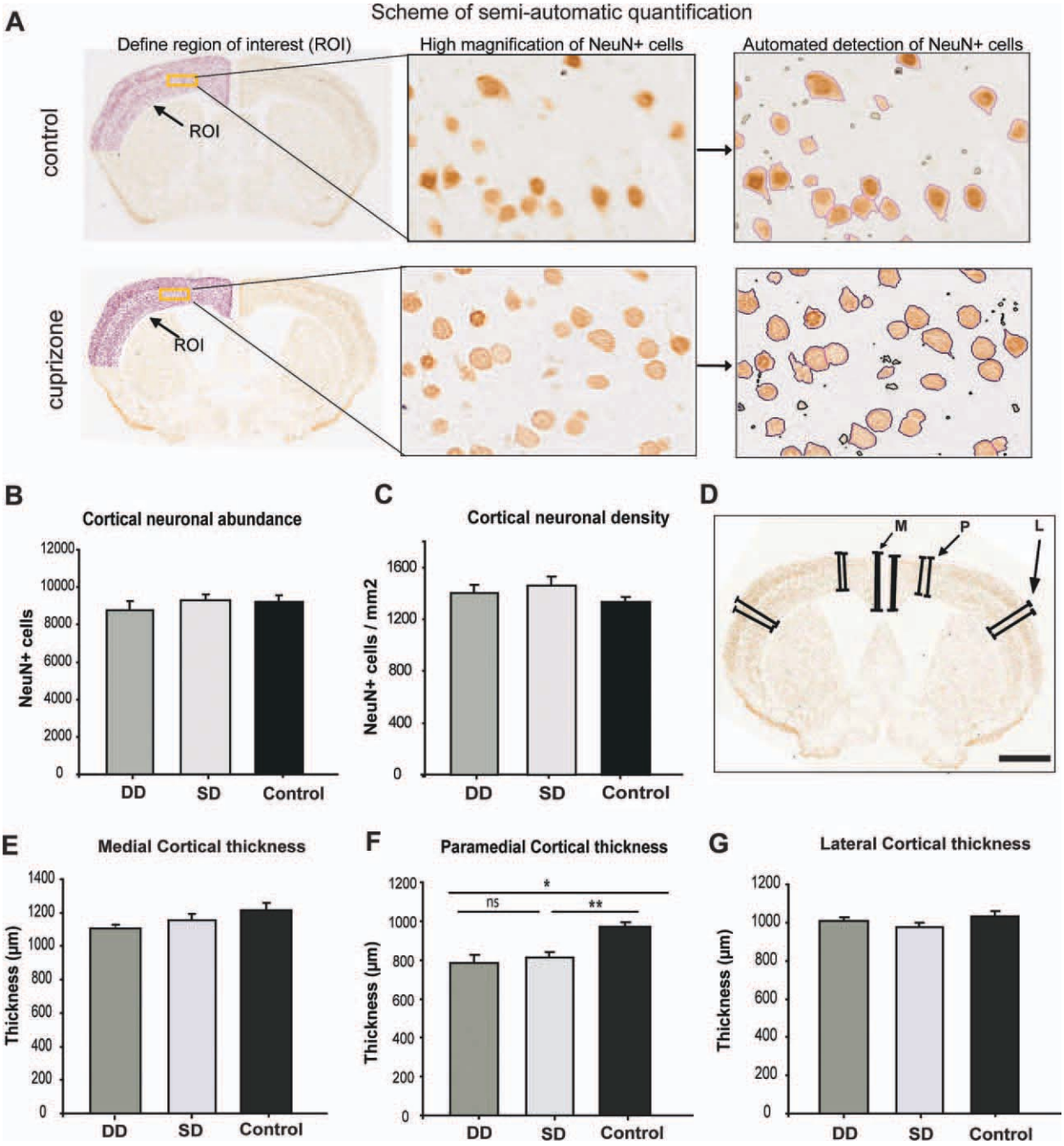

FIGURE 7: NeuN-positive neuronal cell bodies within the cerebral cortex are not lost following 28 weeks after stopping cuprizone treatment. (A) Sections were stained for neuronal nuclei with NeuN antibodies, scanned and automatically counted using Definiens Developer XD software in the indicated ROI. (B) Number of cortical neurons in treated groups and controls are shown as the mean ± SEM. (C) Density of cortical neurons is shown as the mean ± SEM. (D) Scheme showing the different regions where cortical thickness was determined, defined as medial (M), paramedial (P) and lateral (L). Cortical thickness was measured in the medial (E), in the paramedial (F) and the lateral region (G). Bar = 1mm (n = 5–9, error bars represent SEM. Statistically significant differences are indicated by asterisks. If ANOVA indicated significant differences in the main effect ($p < 0.05$), Tukey test pairwise comparison was applied *$p < 0.05$, **$p < 0.01$). ANOVA = analysis of variance; DD = double demyelinated group, ROI = region of interest; SD = single demyelinated group; SEM = standard error of the mean. [Color figure can be viewed in the online issue, which is available at www.annalsofneurology.org.]

mice after 6 weeks of cuprizone feeding followed by 6 weeks of recovery, and from age-matched controls. Relative quantification of the proteome was performed using iTRAQ technology coupled with MS/MS. A total of 240 proteins were detected in ~12-week-old and ~20-month-old mouse myelin and 349 proteins in remyelinated and age-matched control myelin. The principal myelin-associated proteins, MBP, proteolipid

protein (PLP), and 2′,3′-cyclic-nucleotide 3′-phosphodiesterase (CNPase), were identified with the highest protein score, as expected (see Table 1 and Supplementary Tables S1–S3). Mass spectrometry analyses normally result in an overrepresentation of cytosolic proteins because membrane proteins are difficult to detect. We detected a relatively large fraction of membrane-associated proteins (30–32%), including transmembrane (21–24%) and lipid-anchored proteins (7–8%). As expected, the relative abundance of the majority of proteins appeared unaltered after completed remyelination (79% and 87% of proteins presented iTRAQ ratios between 0.8 and 1.2 in aging and remyelination analysis, respectively). The proteins with the largest relative abundance changes are presented in Tables 1 and 2. Interestingly, regression analysis revealed a strong correlation in quantitative changes occurring during aging compared to those observed after remyelination of membrane and membrane-associated proteins (Fig 8), even when including lipid-anchored proteins ($r = 0.77$ for transmembrane proteins and $r = 0.63$ when lipid-anchored proteins and MBP are included, $p < 0.001$ in both cases). Conversely, changes in proteins considered as contamination from myelin purification, such as cytoskeleton/cytoplasm and mitochondrial proteins, presented no correlation ($r = 0.04$ and 0.26, respectively, and $p > 0.5$ in both cases). These data suggest that despite an overall stability in myelin protein composition and relative abundance, subtle changes are evident during aging and remyelination and that these changes seem to have the same tendency for both conditions.

In summary, our findings indicate that late-onset locomotor dysfunction can be observed long after cuprizone-induced demyelination and remyelination. This is accompanied by a reduction of callosal axons and a low level of continuing axonal injury. Furthermore, the restoration of myelin showed changes in the myelin proteome in a pattern similar to that of older animals.

Discussion

We studied the long-term effects of cuprizone-induced demyelination. Motor skills were repeatedly evaluated after remyelination over a period of ~6 months using MOSS.[20] After single or repeated demyelination, animals displayed interim functional recovery with locomotor capacity comparable to controls. However, cuprizone-treated animals displayed late-onset motor impairments, indicating that functional recovery was merely transient and not stable in the long term. Along with these functional deficits, we observed axonal loss despite extensive remyelination.

While axonal damage appears to be critical for clinical disability in chronic progressive MS, the underlying mechanisms are not resolved. Interestingly, neurodegeneration seems to primarily affect neuronal processes, because axonal loss is more frequent than loss of neuronal cell bodies.[48] In this study, cuprizone-induced demyelination caused substantial axonal loss in the corpus callosum without a significant reduction in the numbers of cortical neurons. However, although we could not discover a significant reduction of NeuN-positive neurons in the cortex with this global analysis, it is possible that in a specific neuronal subpopulation, ie, a population not detectable with our approach, the number of NeuN-positive cortical neurons might decrease. With regard to MS, it was shown that specific subpopulations of neurons are more vulnerable to demyelination.[49] We and others found that acute axonal damage is most prominent during cuprizone feeding when demyelination is most extensive.[50–52] Similarly, most APP-positive axons in MS lesions are detected within the first year after disease onset.[6,7] In our model—and probably mechanistically distinct from axonal damage during acute demyelination—ongoing axonal degeneration was evident in remyelinated animals several months after cuprizone was removed from the diet. In addition, APP-positive spheroids were also observed in MS lesions of patients with a disease duration of 10 years and more.[2,6]

These findings raise the question of what underlying factors are contributing to axonal damage and functional impairments in the chronic disease stage long after the demyelinating trigger. Extensive spontaneous repopulation of oligodendrocytes and remyelination is achieved within a few weeks after discontinuation of cuprizone, and axonal damage seems to localize in regions of demyelination and remyelination. Nevertheless, cuprizone could exert long-lasting toxic effects that selectively affect axons in the long term and that may only become apparent at chronic time points. Therefore, we cannot formally rule out the contribution of long-lasting cuprizone effects to axonal degeneration. Similarly, in the current study we cannot exclude the possibility that remyelination was temporarily more complete at the intermediate time point (20 weeks), when full functional recovery was noted. However, previous studies found that after cuprizone was discontinued, a maximal degree of remyelination was achieved within a few weeks and did not substantially change over an observation period of several months.[22,53,54]

A recent study found a close association between axonal degeneration and inflammation even in MS patients with a long disease duration, albeit at a lower level than in acute/RRMS.[12] We also observed a moderate increase of microglia density in remyelinated lesions

TABLE 1: Proteins at 6 Weeks of Recovery with the Largest Relative Abundance Changes Between Myelin After 6 Weeks of Remyelination (R) and Control Samples (C)

Protein Access	Protein Description	Protein Score	iTRAQ Ratio C/R
Top 10 proteins increased in remyelination			
gi|6679186	Claudin 11	1079	0.45
gi|19526794	CD 81 antigen	316	0.47
gi|6680894	CD9 antigen	71	0.47
gi|13173473	Prion protein precursor	112	0.51
gi|84579915	Guanine nucleotide binding protein (G protein), gamma 7	108	0.52
gi|13386338	RAP2B, member of RAS oncogene family precursor	178	0.59
gi|83921618	Villin 2	548	0.60
gi|7305379	Pleckstrin homology domain containing, family B member 1 isoform a	63	0.63
gi|124517716	Solute carrier family 12, member 2	403	0.65
gi|61656194	Sodium channel, type IV, beta precursor	74	0.68
gi|116063560	Contactin associated protein 1 precursor	206	0.68
gi|21450321	Na+/K+ -ATPase alpha 3 subunit	7654	0.70
gi|227499980	Solute carrier family 44, member 1 isoform A	406	0.70
gi|165972315	Related RAS viral (r-ras) oncogene homolog 2 precursor	161	0.70
gi|6671718	CD82 antigen isoform 1	77	0.71
Top 10 decreased in remyelination			
gi|6681195	Postsynaptic density protein 95 isoform 1	116	2.23
gi|6679935	Growth associated protein 43	132	1.75
gi|30409956	Na+/K+ -ATPase alpha 2 subunit precursor	4378	1.58
gi|31560541	Synaptogyrin 3	152	1.56
gi|117606275	Excitatory amino acid transporter 2 isoform 2	297	1.51
gi|24233554	Solute carrier family 1, member 3	195	1.46
gi|51317392	Pleckstrin and Sec7 domain containing homolog	43	1.38
gi|261862282	Solute carrier family 2, member 3	81	1.30
gi|32189434	Immunoglobulin superfamily, member 8	339	1.27
gi|6753074	Adaptor protein complex AP-2, mu1	196	1.25
gi|70778915	Moesin	242	1.24
gi|158711686	Solute carrier family 12, member 5	57	1.24
gi|30725780	MAL2 proteolipid protein	57	1.23
gi|22507355	SOLUTE carrier family 8 (sodium/calcium exchanger), member 2	330	1.20
gi|6753140	Plasma membrane calcium ATPase 2 isoform 1	366	1.15

iTRAQ ratios are depicted for the proteins identified in each analysis.
iTRAQ = isobaric tags for relative and absolute quantitation; C = control; R = remyelination.

TABLE 2: Proteins with the Largest Relative Abundance Changes in Myelin of 12-week-old Mice (Y) Compared to ~20-month-old mice (O)

Protein Access	Protein Description	Protein Score	iTRAQ Ratio Y/O
Top 10 increased in aging			
gi|7305379	Pleckstrin homology domain containing, family B (evectins) member 1 isoform a	61	0.29
gi|162139829	Myelin protein zero precursor	36	0.32
gi|148271067	Myeloid-associated differentiation marker	75	0.37
gi|6679186	Claudin 11	1251	0.45
gi|6680894	CD9 antigen	69	0.51
gi||10947010	Junctophilin 2	30	0.57
gi|227499980	Solute carrier family 44, member 1 isoform A	387	0.65
gi|6671718	CD82 antigen isoform 1	127	0.69
gi|7106349	Ly6/neurotoxin 1 precursor	32	0.74
gi|6754382	CD47 antigen	383	0.74
gi|12963495	Glycoprotein m6b	75	0.76
gi|23956058	Proteolipid protein 1	12245	0.78
gi|89001109	Guanine nucleotide binding protein, alpha 13	260	0.78
gi|30424705	Transmembrane protein 177	41	0.79
gi|47271396	GNAS complex locus XLas	258	0.84
Top 10 decreased in aging			
gi|32189434	Immunoglobulin superfamily, member 8	308	2.60
gi|30409956	Na+/K+ -ATPase alpha 2 subunit precursor	1415	2.51
gi|13384618	Guanine nucleotide binding protein (G protein), gamma 12 precursor	270	2.16
gi|23346547	Cell adhesion molecule 4 precursor	142	1.85
gi|165377226	Solute carrier family 2 (facilitated glucose transporter), member 1	90	1.46
gi|9625037	Ras homolog gene family, member G precursor	214	1.46
gi|266458391	c-K-ras2 protein	231	1.37
gi|10946620	Cell cycle exit and neuronal differentiation 1	92	1.33
gi|12963613	Junction adhesion molecule 3 precursor	184	1.26
gi|13386338	RAP2B, member of RAS oncogene family precursor	63	1.24
gi|113199771	Myelin oligodendrocyte glycoprotein	2844	1.21
gi|6679593	RAB3A, member RAS oncogene family	265	1.19
gi|70608157	Tetraspan 2	183	1.18
gi|45592934	RAS-related C3 botulinum substrate 1 precursor	430	1.18
gi|70778915	Moesin	138	1.17

iTRAQ ratios are depicted for the proteins identified in each analysis.
iTRAQ = isobaric tags for relative and absolute quantitation; O = ~20-month-old mice; Y = 12-week-old mice.

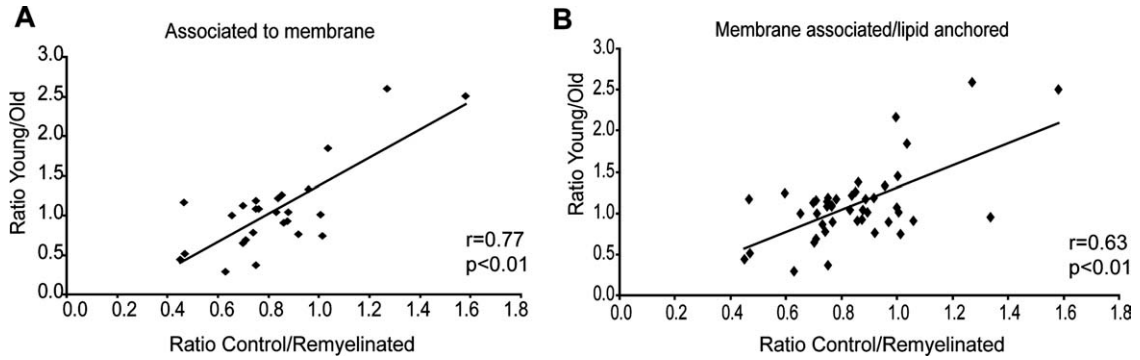

FIGURE 8: Myelin membrane proteome iTRAQ ratios of shared proteins in aging and remyelination. (A) The ratios are shown for membrane-associated proteins (r = 0.77, $p < 0.001$) and (B) lipid-anchored together with membrane-associated proteins (r = 0.63, $p > 0.001$). Regression analysis reveals a strong correlation between changes that occur as a result of aging and remyelination. iTRAQ = isobaric tags for relative and absolute quantitation.

in the animal model and in the MS lesions studied (see Supplementary Fig S1, and data not shown). However, it is still not clear whether this low level of inflammation is the cause or the consequence of ongoing axonal degeneration at these chronic stages. In addition, immunomodulatory therapies have shown little effect in preventing permanent neurological deficits in progressive MS. Thus, in progressive disease stages, inflammation might not be the sole driving force in axonal degeneration.

How such slowly accumulating axonal pathology could contribute to a transition from RRMS to SPMS is still not understood. Early functional recovery from irreversible axonal damage might be achieved by adaptive neuroplasticity mechanisms.[55] However, if axonal degeneration continues at a low level—even in the absence of newly emerging demyelinating insults and/or even after extensive remyelination—the degree of axonal loss could reach a critical threshold at which neuroplastic responses are exhausted and thus progressive clinical symptoms may reappear.[4,56] We propose that even after completed remyelination, axonal degeneration still continues at a low level and accumulates over time, and that once a threshold is passed, axonal degeneration becomes functionally apparent in the long-term. Strikingly, 2 episodes of cuprizone-induced demyelination did not increase or accelerate late-onset functional deterioration compared to a single episode. This might be due to increased resistance to repeated episodes of cuprizone-induced demyelination,[57] but it might also have to do with the age at which animals were last exposed to cuprizone: the SD group received its first and only cuprizone treatment at the same age as the DD group was when it was exposed to cuprizone for the second time (see Fig 1). It was previously reported that axonal damage and loss is more severe when animals are subjected to cuprizone treatment at an older age.[50] Thus, it is possible that, for the functional outcome, the age at the time of the last cuprizone treatment is decisive. At the time of its only cuprizone exposure, the SD group may already have been catching up with the DD group. Interestingly, in MS the number of relapses do not correlate with the severity and time of onset of chronic progressive MS.[58] In fact, age is the most important risk factor for chronic progressive MS.[58] It has been shown that myelin provides the trophic support for axons necessary for their maintenance into late adulthood,[59] and its stability depends on constant remodeling and turnover. However, myelin renewal is not necessarily linked to the preservation of its integrity, as several ultrastructural defects accumulate in the myelin sheath during aging.[60] Some authors even claim that disruption of myelin integrity is related to the cognitive decline observed in aging.[61–63] It has been proposed that the decrease in axonal conduction velocity observed in aging brains[64] and in regions where myelin has been altered[65] affects the transmission of electric signals along the axon, which may disturb normal function in neural circuits necessary for complex behavior and fast response.[60] Ultrastructural changes such as shorter internodes reported during aging suggest an active process of remyelination in the absence of any apparent demyelinating event.[66] In addition, myelin is essential for long-term axonal survival and minor alterations in myelin membrane composition can trigger neurodegeneration.[45–47,59]

It has been reported that the myelin sheath formed after remyelination seems to be ultrastructurally and chemically normal, although it is thinner.[67] In accordance with these findings, we observed that the relative abundance of myelin proteins is unchanged after 6 weeks of remyelination. However, we also found that the subtle changes in the proteome of myelin after remyelination were similar to those of myelin in aged animals. For instance, we observed an increase in relative amount of membrane spanning protein claudin 11 (see Table 1 and 2) following remyelination. This protein is involved in the formation and stabilization of the radial component.

The radial component is thought to modulate the biophysical properties of myelin by providing a diffusion barrier for ions within myelin.[68] Changes in the expression of tight junctions within the radial component may lead to small temporal alteration in nerve transmission. It is also possible that an increased expression of claudin 11, which spans 4 membranes, results in oligodendroglial damage, as was observed in Pelizaeus-Merzbacher disease after overexpression of PLP.[69] Furthermore, claudin 11 is known to be involved in the formation of tight junctions in the radial component of myelin sheaths, as well as in oligodendrocyte proliferation and development.[70] Mice lacking claudin 11 present a slower electric conduction of the axons and their myelin does not contain tight junctions, possibly resulting in diminished insulating properties; absence of claudin 11 results in neurological deficits despite normal compaction.[71]

The present results may provide a source of candidate proteins involved in myelin functional maintenance for use in future studies. However, our analysis does not exclude the possibility that other properties of myelin not detected in our analysis (eg, alteration in posttranslational modification) may account for the observed axonal degeneration in the long term. It is possible that changes in myelin occurring after episodes of demyelination and remyelination are sufficient to induce late-onset neuronal dysfunction which only becomes apparent when mice reach an advanced age. Concomitant with this assumption is our finding that some of the APP-positive axons were ensheathed in myelin 6 months after stopping cuprizone. If changes in myelin content result in impaired axonal trophic support in the long term, inflammatory cells could be recruited secondary to the site of axonal degeneration.

It should be mentioned that numerous studies provide evidence that remyelination is advantageous for axonal function. Replacement of damaged myelin not only restores nerve conduction[72] but also provides a neuroprotective function by reducing axonal degeneration.[51] The beneficial function of myelin has been shown in numerous studies and is undisputed.[11,51,73–75] However, the current data indicate that minor alterations accumulating in remyelinated myelin can result in subtle changes in axonal function that may only become functionally relevant in the long term. Whether any of these important functions are lost in older animals after inducing episodes of demyelination and remyelination is an important question that must be addressed in future studies.

In summary, cuprizone-induced demyelination results in temporary functional recovery but at a later time point leads to late-onset motor impairment. Novel therapeutic approaches for neuroprotection not only need to reduce acute but also long-term axonal damage. The model presented here mimics some of the aspects of axonal pathology observed in chronic progressive MS and might therefore be useful, not only to study the factors triggering and maintaining long-lasting axonal damage, but also to evaluate neuroprotective treatment strategies.

Acknowledgments

This work was supported by a European Research Council Starting Grant (Project No: 204034) and the EMBO YIP (to M.S.), a Göttingen Graduate School for Neurosciences and Molecular Neurosciences (GNNB) Excellence Stipend (to N.M-H.), and a grant from the DFG (SFB Transregio 43 to D.M. and W.B.), and is further supported by the Swiss National Science Foundation (PP00P3_128372 to D.M.).

We thank Andrew Woehler for comments on the manuscript and Christine Crozier and Cynthia Bunker for language editing. We thank Dr. Jack Antel (Neuroimmunology Unit, Montreal Neurological Institute, McGill Montreal) for providing MS tissue samples.

Potential Conflicts of Interest

W.B.: grants: consultancy: Teva Pharma, BiogenIdec, Novartis; grants/grants pending: Teva Pharma, Novartis, BiogenIdec, Bayer Schering; Payment for lectures including service on speakers bureaus: Teva Pharma, BiogenIdec, Bayer Schering, Sanofi-Aventis, Merck-Serono, Novartis; travel/accommodations/meeting expenses unrelated to activities listed: Teva Pharma, Sanofi-Aventis, BiogenIdec, Bayer Schering, Merck-Serono, Novartis. T.K.: consultancy: BayerHealthCare; payment for lectures including service on speakers bureaus: Teva, BayerVital, Bayer HealthCare, MerckSerono, SeronoSymposia International Foundation; M.S. travel support: BayerHealthCare, Teva, Novartis, Merck-Serono.

References

1. Friese MA, Montalban X, Willcox N, et al. The value of animal models for drug development in multiple sclerosis. Brain 2006; 129:1940–1952.
2. Trapp BD, Peterson J, Ransohoff RM, et al. Axonal transection in the lesions of multiple sclerosis. N Engl J Med 1998;338:278–285.
3. Noseworthy JH, Lucchinetti C, Rodriguez M, Weinshenker BG. Multiple sclerosis. N Engl J Med 2000;343:938–952.
4. Bjartmar C, Trapp B. Axonal degeneration and progressive neurologic disability in multiple sclerosis. Neurotox Res 2003;5: 157–164.
5. Compston A, Coles A. Multiple sclerosis. Lancet 2008;372: 1502–1517.
6. Kuhlmann T, Lingfeld G, Bitsch A, et al. Acute axonal damage in multiple sclerosis is most extensive in early disease stages and decreases over time. Brain 2002;125:2202–2212.

7. Bitsch A, Schuchardt J, Bunkowski S, et al. Acute axonal injury in multiple sclerosis: correlation with demyelination and inflammation. Brain 2000;123:1174–1183.
8. Ferguson B, Matyszak MK, Esiri MM, Perry VH. Axonal damage in acute multiple sclerosis lesions. Brain 1997;120:393–399.
9. Kornek B, Storch MK, Weissert R, et al. Multiple sclerosis and chronic autoimmune encephalomyelitis : a comparative quantitative study of axonal injury in active, inactive, and remyelinated lesions. Am J Pathol 2000;157:267–276.
10. Brück W, Kuhlmann T, Stadelmann C. Remyelination in multiple sclerosis. J Neurol Sci 2003;206:181–185.
11. Franklin RJM, ffrench-Constant C. Remyelination in the CNS: from biology to therapy. Nat Rev Neurosci 2008;9:839–855.
12. Frischer JM, Bramow S, Dal-Bianco A, et al. The relation between inflammation and neurodegeneration in multiple sclerosis brains. Brain 2009;132:1175–1189.
13. Miller DH, Leary SM. Primary-progressive multiple sclerosis. Lancet Neurol 2007;6:903–912.
14. Leary SM, Thompson AJ. Primary progressive multiple sclerosis: current and future treatment options. 19 vol. Auckland, New Zealand: Adis International, 2005:8.
15. Kremenchutzky M, Rice GPA, Baskerville J, et al. The natural history of multiple sclerosis: a geographically based study 9: observations on the progressive phase of the disease. Brain 2006; 129:584–594.
16. Vukusic S, Confavreux C. Natural history of multiple sclerosis: risk factors and prognostic indicators. Curr Opin Neurol 2007;20: 269–274.
17. Matsushima GK, Morell P. The neurotoxicant, cuprizone, as a model to study demyelination and remyelination in the central nervous system. Brain Pathol 2001;11:107–116.
18. Blakemore WF. Demyelination of the superior cerebellar peduncle in the mouse induced by cuprizone. J Neurol Sci 1973;20:63–72.
19. Blakemore WF, Franklin RJM. Remyelination in experimental models of toxin-induced demyelination. In: Advances in multiple sclerosis and experimental demyelinating diseases. Curr Top Microbiol Immunol, 2008;193–212.
20. Liebetanz D, Merkler D. Effects of commissural de- and remyelination on motor skill behaviour in the cuprizone mouse model of multiple sclerosis. Exp Neurol 2006;202:217–224.
21. Merkler D, Boretius S, Stadelmann C, et al. Multicontrast MRI of remyelination in the central nervous system. NMR Biomed 2005; 18:395–403.
22. Mason JL, Langaman C, Morell P, et al. Episodic demyelination and subsequent remyelination within the murine central nervous system: changes in axonal calibre. Neuropathol Appl Neurobiol 2001;27:50–58.
23. Hiremath MM, Saito Y, Knapp GW, et al. Microglial/macrophage accumulation during cuprizone-induced demyelination in C57BL/6 mice. J Neuroimmunol 1998;92:38–49.
24. Nikić I, Merkler D, Sorbara C, et al. A reversible form of axon damage in experimental autoimmune encephalomyelitis and multiple sclerosis. Nat Med 2011;17:495–499.
25. Coetzee T, Fujita N, Dupree J, et al. Myelination in the absence of galactocerebroside and sulfatide: normal structure with abnormal function and regional instability. Cell 1996;86:209–219.
26. Norton WT, Poduslo SE. Myelination of rat brain: method of myelin isolation. J Neurochem 1973;21:749–757.
27. Bradford MM. A rapid and sensitive method for the quantitation of microgram quantities of protein utilizing the principle of protein-dye binding. Anal Biochem 1976;72:248–254.
28. Thingholm TE, Larsen MR. The use of titanium dioxide micro-columns to selectively isolate phosphopeptides from proteolytic digests. In: de Graauw M, ed. Phospho-proteomics. Methods in Molecular Biology™. Vol. 527. New York: Humana Press, 2009: 57–66.
29. Pruitt KD, Tatusova T, Maglott DR. NCBI Reference Sequence Project: update and current status. Nucleic Acids Res 2003;31:34–37.
30. Perkins DN, Pappin DJC, Creasy DM, Cottrell JS. Probability-based protein identification by searching sequence databases using mass spectrometry data. Electrophoresis 1999;20: 3551–3567.
31. Guo Y, Singleton PA, Rowshan A, et al. Quantitative proteomics analysis of human endothelial cell membrane rafts. Mol Cell Proteomics 2007;6:689–696.
32. Martin B, Brenneman R, Becker KG, et al. iTRAQ analysis of complex proteome alterations in 3xTgAD Alzheimer's mice: understanding the interface between physiology and disease. PLoS One 2008;3:e2750.
33. Kassie F, Anderson LB, Higgins L, et al. Chemopreventive agents modulate the protein expression profile of 4-(methylnitrosamino)-1-(3-pyridyl)-1-butanone plus benzo[a]pyrene-induced lung tumors in A/J mice. Carcinogenesis 2008;29:610–619.
34. Graham R, Sharma M, Ternan N, et al. A semi-quantitative GeLC-MS analysis of temporal proteome expression in the emerging nosocomial pathogen Ochrobactrum anthropi. Genome Biol 2007;8:R110.
35. The UniProt Consortium. The Universal Protein Resource (UniProt). Nucleic Acids Res 2008;36:D190–D195.
36. Krogh A, Larsson B, von Heijne G, Sonnhammer ELL. Predicting transmembrane protein topology with a hidden Markov model: application to complete genomes. J Mol Biol 2001;305:567–580.
37. Käll L, Krogh A, Sonnhammer ELL. A combined transmembrane topology and signal peptide prediction method. J Mol Biol 2004; 338:1027–1036.
38. Hibbits N, Pannu R, Wu TJ, Armstrong RC. Cuprizone demyelination of the corpus callosum in mice correlates with altered social interaction and impaired bilateral sensorimotor coordination. ASN Neuro 2009;1pii:e00013.
39. Schalomon PM, Wahlsten D. Wheel running behavior is impaired by both surgical section and genetic absence of the mouse corpus callosum. Brain Res Bull 2002;57:27–33.
40. Hirano A. The role of electron microscopy in neuropathology. Acta Neuropathol 2005;109:115–123.
41. Grassiot B, Desgranges B, Eustache F, Defer G. Quantification and clinical relevance of brain atrophy in multiple sclerosis: a review. J Neurol 2009;256:1397–1412.
42. Siffrin V, Vogt J, Radbruch H, et al. Multiple sclerosis—candidate mechanisms underlying CNS atrophy. Trends Neurosci 2010;33:202–210.
43. Kutzelnigg A, Lassmann H. Cortical lesions and brain atrophy in MS. J Neurol Sci 2005;233:55–59.
44. Miller DH, Barkhof F, Frank JA, et al. Measurement of atrophy in multiple sclerosis: pathological basis, methodological aspects and clinical relevance. Brain 2002;125:1676–1695.
45. Lappe-Siefke C, Goebbels S, Gravel M, et al. Disruption of Cnp1 uncouples oligodendroglial functions in axonal support and myelination. Nat Genet 2003;33:366–374.
46. Griffiths I, Klugmann M, Anderson T, et al. Axonal swellings and degeneration in mice lacking the major proteolipid of myelin. Science 1998;280:1610–1613.
47. Yin X, Crawford TO, Griffin JW, et al. Myelin-associated glycoprotein is a myelin signal that modulates the caliber of myelinated axons. J. Neurosci 1998;18:1953–1962.
48. Trapp BD, Nave K-A. Multiple sclerosis: an immune or neurodegenerative disorder? Ann Rev Neurosci 2008;31:247–269.
49. Clements R, McDonough J, Freeman E. Distribution of parvalbumin and calretinin immunoreactive interneurons in motor cortex from multiple sclerosis post-mortem tissue. Exp Brain Res 2008;187: 459–465.

50. Irvine KA, Blakemore WF. Age increases axon loss associated with primary demyelination in cuprizone-induced demyelination in C57BL/6 mice. J Neuroimmunol 2006;175:69–76.
51. Irvine KA, Blakemore WF. Remyelination protects axons from demyelination-associated axon degeneration. Brain 2008;131: 1464–1477.
52. Lindner M, Fokuhl J, Linsmeier F, et al. Chronic toxic demyelination in the central nervous system leads to axonal damage despite remyelination. Neurosci Lett 2009;453:120–125.
53. Lindner M, Heine S, Haastert K, et al. Sequential myelin protein expression during remyelination reveals fast and efficient repair after central nervous system demyelination. Neuropathol Appl Neurobiol 2008;34:105–114..
54. Ludwin SK, Maitland M. Long-term remyelination fails to reconstitute normal thickness of central myelin sheaths. J Neurol Sci 1984; 64:193–198.
55. Kerschensteiner M, Bareyre FM, Buddeberg BS, et al. Remodeling of axonal connections contributes to recovery in an animal model of multiple sclerosis. J Exp Med 2004;200:1027–1038.
56. Trapp BD, Ransohoff RM, Fisher E, Rudick RA. Neurodegeneration in multiple sclerosis: relationship to neurological disability. Neuroscientist 1999;5:48–57.
57. Johnson ES, Ludwin SK. The demonstration of recurrent demyelination and remyelination of axons in the central nervous system. Acta Neuropathol 1981;53:93–98.
58. Confavreux C, Vukusic S, Moreau T, Adeleine P. Relapses and progression of disability in multiple sclerosis. N Engl J Med 2000; 343:1430–1438.
59. Nave K-A, Trapp BD. Axon-glial signaling and the glial support of axon function. Ann Rev Neurosci 2008;31:535–561.
60. Peters A. The effects of normal aging on myelin and nerve fibers: a review. J Neurocytol 2002;31:581–593.
61. Peters A, Morrison JH, Rosene DL, Hyman BT. Are neurons lost from the primate cerebral cortex during normal aging? Cereb Cortex 1998;8:295–300.
62. Peters A. Age-related changes in oligodendrocytes in monkey cerebral cortex. J Comp Neurol 1996;371:153–163.
63. Bartzokis G. Age-related myelin breakdown: a developmental model of cognitive decline and Alzheimer's disease. Neurobiol Aging 2004;25:5–18.
64. Xi MC, Liu RH, Engelhardt JK, et al. Changes in the axonal conduction velocity of pyramidal tract neurons in the aged cat. Neuroscience 1999;92:219–225.
65. Felts PA, Baker TA, Smith KJ. Conduction in segmentally demyelinated mammalian central axons. J Neurosci 1997;17: 7267–7277.
66. Lasiene J, Matsui A, Sawa Y, et al. Age-related myelin dynamics revealed by increased oligodendrogenesis and short internodes. Aging Cell 2009;8:201–213.
67. Ludwin SK, Sternberger NH. An immunohistochemical study of myelin proteins during remyelination in the central nervous system. Acta Neuropathol 1984;63:240–248.
68. Devaux J, Gow A. Tight junctions potentiate the insulative properties of small CNS myelinated axons. J Cell Biol 2008;183: 909–921.
69. Yool DA, Edgar JM, Montague P, Malcolm S. The proteolipid protein gene and myelin disorders in man and animal models. Hum Mol Genet 2000;9:987–992.
70. Bronstein JM, Chen K, Tiwari-Woodruff S, Kornblum HI. Developmental expression of OSP/claudin-11. J Neurosci Res 2000;60: 284–290.
71. Gow A, Southwood CM, Li JS, et al. CNS myelin and sertoli cell tight junction strands are absent in Osp/Claudin-11 null mice. Cell 1999;99:649–659.
72. Smith KJ, Blakemore WF, McDonald WI. Central remyelination restores secure conduction. Nature 1979;280:395–396.
73. Duncan ID, Brower A, Kondo Y, et al. Extensive remyelination of the CNS leads to functional recovery. Proc Natl Acad Sci U S A 2009;106:6832–6836.
74. Piaton G, Gould RM, Lubetzki C. Axon-oligodendrocyte interactions during developmental myelination, demyelination and repair. J Neurochem 2010;114:1243–1260.
75. Taveggia C, Feltri ML, Wrabetz L. Signals to promote myelin formation and repair. Nat Rev Neurol 2010;6:276–287